

# Correction of the Sea State Impact in the L-Band Brightness Temperature by Means of Delay-Doppler Maps of Global Navigation Satellite Signals Reflected Over the Sea Surface

Juan Fernando Marchán-Hernández, *Student Member, IEEE*, Nereida Rodríguez-Álvarez, *Student Member, IEEE*, Adriano Camps, *Senior Member, IEEE*, Xavier Bosch-Lluis, *Student Member, IEEE*, Isaac Ramos-Pérez, *Associate Member, IEEE*, and Enric Valencia, *Student Member, IEEE*

**Abstract**—This paper presents an efficient procedure based on 2-D convolutions to obtain delay-Doppler maps (DDMs) of Global Navigation Satellite Signals reflected (GNSS-R) over the sea surface and collected by a spaceborne receiver. Two DDM-derived observables (area and volume) are proposed to link the sea-state-induced brightness temperature to the measured normalized DDM. Finally, the requirements to use Global Positioning System reflectometry to accurately correct for the sea state impact on the L-band brightness temperature (quantization levels, decimation, truncation, and noise impact) are analyzed in view of its implementation in the Passive Advanced Unit instrument of the Spanish Earth Observation Satellite (SeoSAT/INGENIO) project.

**Index Terms**—Brightness temperature, Delay-Doppler Map (DDM), Global Navigation Satellite Systems (GNSSs), sea state.

## I. INTRODUCTION

IT IS GENERALLY accepted that the best way to retrieve sea surface salinity (SSS) is by means of L-band radiometry (1400–1427 MHz). However, in addition to polarization “p,” incidence angle  $\theta$ , SSS, and sea surface temperature (SST), sea surface brightness temperature  $T_B$  depends on the sea state, which is the largest contributor to the deviations of the brightness temperature with respect to the flat sea model [1], i.e.,

$$T_{B,p}(\theta) = T_{B,p,\text{flat sea}}(\theta, f, \text{SSS}, \text{SST}) + \Delta T_{B,p}(\theta, \vec{p})$$

where  $\vec{p}$  is a generic vector of parameters that define the sea state. The sea state is usually parameterized in terms of the

10-m height wind speed  $U_{10}$  and/or the significant wave height (SWH) [2], [3], but none of them are fully satisfactory.

The use of Global Navigation Satellite System (GNSS) signals reflected by the sea surface for altimetry applications was first suggested by Martín-Neira [4] and, more recently, for sea state determination using the so-called “waveforms” [5]–[7]. These retrievals have been performed using ground-based [8], airborne [5], and stratospheric sensors [9]. The GNSS reflected (GNSS-R) approach has also been used to perform soil moisture retrieval [10] and ice characterization [11]. The global coverage offered by the spaceborne platforms [12], [13] has allowed to study several geophysical parameters (e.g., salinity, soil moisture, and ice) with the same sensor. In this paper, we advance in the use of the full delay-Doppler map (DDM) defined in Section II to make the necessary sea state  $T_B$  corrections ( $\Delta T_{B,p}(\theta, \vec{p})$ ) in SSS retrieval algorithms.

The Global Positioning System was designed to provide global positioning at any time. To achieve this goal, a minimum of four satellites is required to simultaneously be visible. The GPS constellation is formed by at least four satellites in each of the six orbital planes phased  $60^\circ$  [14]. The orbits are near circular and have an inclination of  $55^\circ$ , a semimajor axis of approximately 26 562 km, and an orbital period of about 12 h. The so-called Standard Positioning Service (SPS) is a positioning and timing service provided at the GPS L1 band (1575.42 MHz). Each GPS satellite transmits in this band a signal that contains a pseudorandom noise coarse/acquisition (C/A) code that is unique and known for each satellite plus the navigation message. It also contains a precision code (P) that is reserved for military uses, but this is not part of the SPS. A new civil signal in L2 (LC2) is already being transmitted from the new GPS satellites. The spreading code used differs from the C/A one, but it could similarly be employed to obtain and process DDM sea state corrections.

The GPS signal is transmitted using a right-hand circularly polarized electromagnetic wave that, when scattered over the sea surface, becomes left-hand elliptically polarized. Over a perfectly calm (flat) sea, the scattered signal comes from the specular reflection point, which is determined by the shortest distance between the transmitting GPS satellite and the receiver. However, when the sea is roughed, the scattered signals come

Manuscript received October 15, 2007; revised March 5, 2008. Current version published October 1, 2008. This work, conducted as part of the award “Passive Advanced Unit (PAU): A Hybrid L-band Radiometer, GNSS-Reflectometer and IR-Radiometer for Passive Remote Sensing of the Ocean” made under the European Heads of Research Councils and European Science Foundation European Young Investigator (EURYI) Awards scheme in 2004, was supported in part by the Participating Organizations of EURYI, by the EC Sixth Framework Program, by the Department of Universities of the Catalan Autonomous Government, by the European Social Fund, and by Spanish Plan Nacional del Espacio project PAU in SeoSAT.

The authors are with the Remote Sensing Laboratory, Department of Signal Theory and Communications, Universitat Politècnica de Catalunya (UPC), 08034 Barcelona, Spain and the IEEC CRAE/UPC.

Color versions of one or more of the figures in this paper are available online at <http://ieeexplore.ieee.org>.

Digital Object Identifier 10.1109/TGRS.2008.922144

from a wider region that enlarges with increasing sea state, in a similar manner as the sun reflecting over the sea surface. If the scattering surface is a plane, the loci of constant delay (isorange) are a set of ellipses, and the loci of constant Doppler shift (isoDoppler) are a set of hyperbolae.<sup>1</sup> Therefore, each point over the surface has a particular delay and Doppler (actually there are two points with the same delay and Doppler). In radar, the ambiguity function [15] provides a measure of the similitude between a signal and a delayed version of it that may include a Doppler shift. In GNSS-R, the equivalent of the ambiguity function in radar is known as a DDM and consists of the power distribution of the reflected signal over the 2-D space of delay offsets and Doppler shifts. Therefore, the shape of the DDM is actually providing a measurement of the size of the area over which the GPS signals are scattered (which is also known as the *glistening zone*). Thus, larger sizes mean that the received signal is composed by contributions from a wider range of propagation delays and Doppler shifts.

The basic idea of this work is to use this property to estimate the sea state and to make the necessary corrections in the L-band brightness temperature to retrieve SSS with an improved accuracy. This work has been performed during phase A of the proposed Passive Advanced Unit (PAU)<sup>2</sup> in Spanish Earth Observation Satellite (SeoSAT/INGENIO)<sup>3</sup> secondary scientific instrument. PAU in SeoSAT is a simplified version of the PAU instrument under development with funds from the European Science Foundation. It is a hybrid pseudocorrelation radiometer at 1400–1427 MHz and GPS reflectometer (1575.42 MHz), following the concept described in [16] but with only one receiver and a left-hand circularly polarized antenna with a 25° beamwidth.

This paper is organized as follows: Section II describes an efficient technique to compute the DDMs as measured from a satellite-borne receiver. Section III presents the relationship between the brightness temperature and two DDM-derived observables. Section IV presents some practical aspects that may limit the performance of this technique: the size of the DDM, the resolution in delay and Doppler, the quantization effects, and the measurement noise. Finally, Section V summarizes the main conclusions of this paper.

## II. SIMULATION OF DDMs

In order to compute the DDMs, it is necessary to know the scattering geometry: the positions of the GNSS-R receiver and the GPS satellites (Fig. 1). Assuming the spherical Earth, the incidence  $\theta_i$  and scattering  $\theta_s$  angles at a given pixel from GPS satellites toward the GNSS-R receiver are computed as

$$\theta_i = \arccos(-\hat{r} \cdot \hat{n}_i) \quad (1a)$$

$$\theta_s = \arccos(\hat{r} \cdot \hat{n}_s) \quad (1b)$$

<sup>1</sup>If the scattering surface is not a plane, as it is the Earth's surface, these curves are no longer ellipses and hyperbolae, and have more complicated expressions.

<sup>2</sup>PAU is an instrument concept for ocean monitoring that was awarded an EURYI Award from the European Science Foundation in 2004.

<sup>3</sup>The E.O. SeoSAT/INGENIO satellite is the Spanish contribution to GMES.

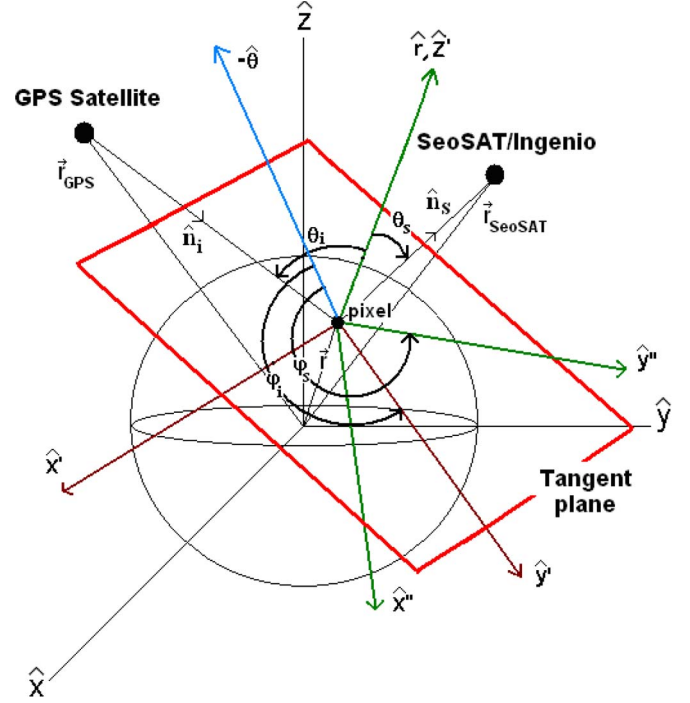


Fig. 1. Scattering geometry and definition of variables.

where  $\hat{r} = \vec{r}/|\vec{r}|$  is the unitary vector perpendicular to the tangent plane at the pixel position,  $\vec{r}_{\text{GPS}}$  is the GPS satellite position,  $\vec{r}_{\text{SeoSAT}}$  is the SeoSAT satellite position,  $\hat{n}_i = (\vec{r} - \vec{r}_{\text{GPS}})/|(\vec{r} - \vec{r}_{\text{GPS}})|$  and  $\hat{n}_s = -(\vec{r} - \vec{r}_{\text{SeoSAT}})/|(\vec{r} - \vec{r}_{\text{SeoSAT}})|$  are the unitary vectors from the GPS satellite to the pixel and from the pixel to the GNSS-R receiver satellite, and  $\vec{r}$  is the pixel position.

Similarly, the azimuth angles with respect to the north are computed as

$$\varphi_i = \arccos(-\hat{\theta} \cdot \hat{y}') \quad (2a)$$

$$\varphi_s = \arccos(-\hat{\theta} \cdot \hat{y}'') \quad (2b)$$

where  $-\hat{\theta}$  is the normalized vector at the pixel tangent to the earth's surface and pointing toward the north; and  $\hat{y}'$  and  $\hat{y}''$  are the normalized projections of  $\hat{n}_i$  and  $\hat{n}_s$ , respectively, over the tangent plane. To solve the ambiguity due to the arccos function, the dot product with respect to  $\hat{x}'$  and  $\hat{x}''$  is also computed.<sup>4</sup>

Once the geometry is known, following Zavorotny's notation [10]–[12], the average power of the reflected GPS signal (DDM) can be expressed as follows:

$$\langle |Y(\tau, f_d)|^2 \rangle = T_i^2 \iint_G \frac{|\Re|^2 D^2(\vec{\rho}) \Lambda^2(\Delta\tau) |S(\Delta f)|^2}{4\pi R_0^2(\vec{\rho}) R^2(\vec{\rho})} \times \frac{q^4(\vec{\rho})}{q_z^4(\vec{\rho})} P_v \left( -\frac{\vec{q}_\perp}{q_z} \right) d^2\rho \quad (3)$$

where  $T_i$  is the coherent integration time;  $\tau$  is the delay;  $f_d$  is the Doppler frequency;  $\Delta\tau = \tau - \tau(\vec{\rho})$ ;  $\Delta f = f_d - f_d(\vec{\rho})$ ;  $\vec{\rho}$  is the position vector of a surface point;  $\tau(\vec{\rho})$  and  $f_d(\vec{\rho})$

<sup>4</sup> $\psi_i = \arccos(-\hat{\theta} \cdot \hat{x}')$ , and  $\psi_s = \arccos(-\hat{\theta} \cdot \hat{x}'')$ , recalling that  $\varphi_{i,s}$  and  $\psi_{i,s}$  are 90° apart.

are the delay offset and Doppler shift associated to a signal contribution reflected at the surface point  $\vec{\rho}$ , respectively;  $\mathfrak{R}$  is the Fresnel reflection coefficient at a given polarization;  $D$  is the antenna radiation pattern;  $R_0$  is the distance from the GPS transmitter to the scattering point;  $R$  is the distance from this point to the receiver;  $\vec{q}$  is the scattering vector defined as  $\vec{q} = \hat{n}_s - \hat{n}_i$ ;  $q \hat{=} |\vec{q}|$ ;  $\vec{q} \hat{=} \vec{q}_\perp + q_z \hat{z}$ ;  $P_\sigma$  is the probability of having a given sea surface slope;  $G$  is the integration domain (the space coordinates of the sea surface); and the  $\Lambda$  and  $|S|$  functions are defined as  $\Lambda = 1 - |\tau|/\tau_c$  if  $|\tau| \leq \tau_c$  and 0 elsewhere ( $\tau_c$  is the length of a chip of the C/A code and has a length of 1 ms/1023); and  $|S(f)| = |\sin(\pi f)/(\pi f)|$ .

The integral in (3) is performed over  $G$ , i.e., the area from where there are contributions to the received signal. The numerical implementation of this equation is a bottleneck to simulate DDMs since, for a satellite-borne GNSS-R receiver, the zone extends over hundreds of kilometers ( $\sim 240$  km of diameter for  $U_{10} = 4$  m/s and  $\sim 400$  km for  $U_{10} = 10$  m/s at nadir incidence) and the number of sampling points becomes very large. To easily perform the numerical integration, it is useful to consider that both  $\Lambda$  and  $|S|$  can be expressed as [18]

$$\Lambda^2(\tau - \beta) = \int_{-\infty}^{+\infty} \Lambda^2(\tau - \gamma) \cdot \delta(\gamma - \beta) d\gamma \quad (4)$$

$$|S(f_d - \varepsilon)|^2 = \int_{-\infty}^{+\infty} |S(f_d - \eta)|^2 \delta(\eta - \varepsilon) d\eta \quad (5)$$

where  $\delta(\cdot)$  is the Dirac delta function. Substituting (4) and (5) into (3) yields

$$\begin{aligned} & \langle |Y(\tau, f_d)|^2 \rangle \\ &= T_i^2 \iint_G \frac{D^2(\vec{\rho})}{4\pi R_0^2(\vec{\rho}) R^2(\vec{\rho})} \left( \int_{-\infty}^{+\infty} \Lambda^2(\tau - \gamma) \delta(\gamma - \beta) d\gamma \right) \\ & \cdot \left( \int_{-\infty}^{+\infty} |S(f_d - \eta)|^2 \delta(\eta - \varepsilon) d\eta \right) \sigma^0(\vec{\rho}) d^2\rho. \quad (6) \end{aligned}$$

Rearranging the terms inside the double integral

$$\begin{aligned} & \langle |Y(\tau, f_d)|^2 \rangle \\ &= \int_{-\infty}^{+\infty} \int_{-\infty}^{+\infty} \Lambda^2(\tau - \gamma) |S(f_d - \eta)|^2 \\ & \cdot \left( T_i^2 \iint_G \frac{D^2(\vec{\rho}) \sigma^0(\vec{\rho})}{4\pi R_0^2(\vec{\rho}) R^2(\vec{\rho})} \right. \\ & \quad \left. \times \delta(\gamma - \tau(\vec{\rho})) \delta(\eta - f_d(\vec{\rho})) d^2\rho \right) d\eta \cdot d\gamma \quad (7) \end{aligned}$$

where  $c$  is the speed of light, and  $\beta$  and  $\varepsilon$  in (4) and (5) have been substituted by  $\tau(\vec{\rho})$  and  $f_d(\vec{\rho})$ , respectively. The preceding

equation can be expressed as a 2-D convolution

$$\langle |Y(\tau, f_d)|^2 \rangle = \chi^2(\tau, f_d) ** \Sigma(\tau, f_d) \quad (8)$$

where  $\chi$  is the ambiguity function in radar terminology, which is independent on the pixel position and easy to compute. The ambiguity function can be understood as the impulse response to the scattered signal from a single delay-Doppler cell. On the other hand,  $\Sigma$  is given by

$$\begin{aligned} \Sigma(\tau, f_d) = T_i^2 \iint_G & \frac{D^2(\vec{\rho}) \sigma^0(\vec{\rho})}{4\pi R_0^2(\vec{\rho}) R^2(\vec{\rho})} \\ & \times \delta(\tau - \tau(\vec{\rho})) \delta(f_d - f_d(\vec{\rho})) d^2\rho \quad (9) \end{aligned}$$

and accounts for the surface geometry, the antenna patterns, and other constants from the bistatic radar equation, assigning a “weighting factor” to each delay-Doppler cell of the scene. To compute  $\Sigma$ , a bidimensional Cartesian  $x$ - $y$  space is first defined, and the delay and Doppler values, the bistatic scattering coefficient, the antenna pattern contribution, and the propagation losses are computed at each  $(x, y)$  point using geometrical relationships. Finally, the  $(x, y)$  points associated to a delay-Doppler cell  $(\tau, f_d)$  are all added.

The simulation results presented have been obtained with a PAU/SeoSAT simulator. This simulator has been implemented in Matlab and allows one to create an Earth scenario composed of GPS satellites broadcasting over the Earth and another satellite (SeoSAT/INGENIO in this particular case) receiving the reflections and computing the DDMs for the different GPS satellites. The SeoSAT satellite’s orbit is not yet determined at the time of performing this study, but a polar (inclination = 98.9°) circular orbit with a height of 681 km ( $v = 7.5$  km/s) has been assumed. The orbital elements of the GPS satellites have been obtained from data<sup>5</sup> given by the “Center for Space, Standard and Innovation” and the GPS satellites, and SeoSAT relative geometry is computed in 20-s steps. PAU’s antenna consists of a seven-patch hexagonal array with a beamwidth ( $-3$  dB) of  $\sim 25^\circ$ , providing a footprint of  $\sim 260$  km, which best matches the glistening zone at medium wind speeds. Fig. 2(a) and (b) shows the computed DDMs (steps  $\Delta\tau = 1$  chip and  $\Delta f_d = 500$  Hz) for wind speeds equal to 3 and 10 m/s in the particular case that the GPS satellite is exactly located in the zenith of the GPS receiver. A logarithmic scale has been used to better show how the tails of the function extend toward higher delays when the sea surface roughness increases. Note that the envelope (the border between the bins with and without power contribution) is the same in both cases, but in the second one [Fig. 2(b)], the tails extend over a longer area. Fig. 3(a) and (b) shows the DDMs computed for the same wind speeds, as shown in Fig. 2(a) and (b), respectively. In this case, the GPS scattered signal is not at nadir position but at  $12^\circ$  off-nadir. As it can be appreciated, the symmetry is now broken, and one tail is larger than the other. The shape of the envelope in Fig. 3(a) and (b) is the same, but it is different from Fig. 2(a) and (b) since it is only determined by geometrical factors.

<sup>5</sup><http://celestrak.com/>.

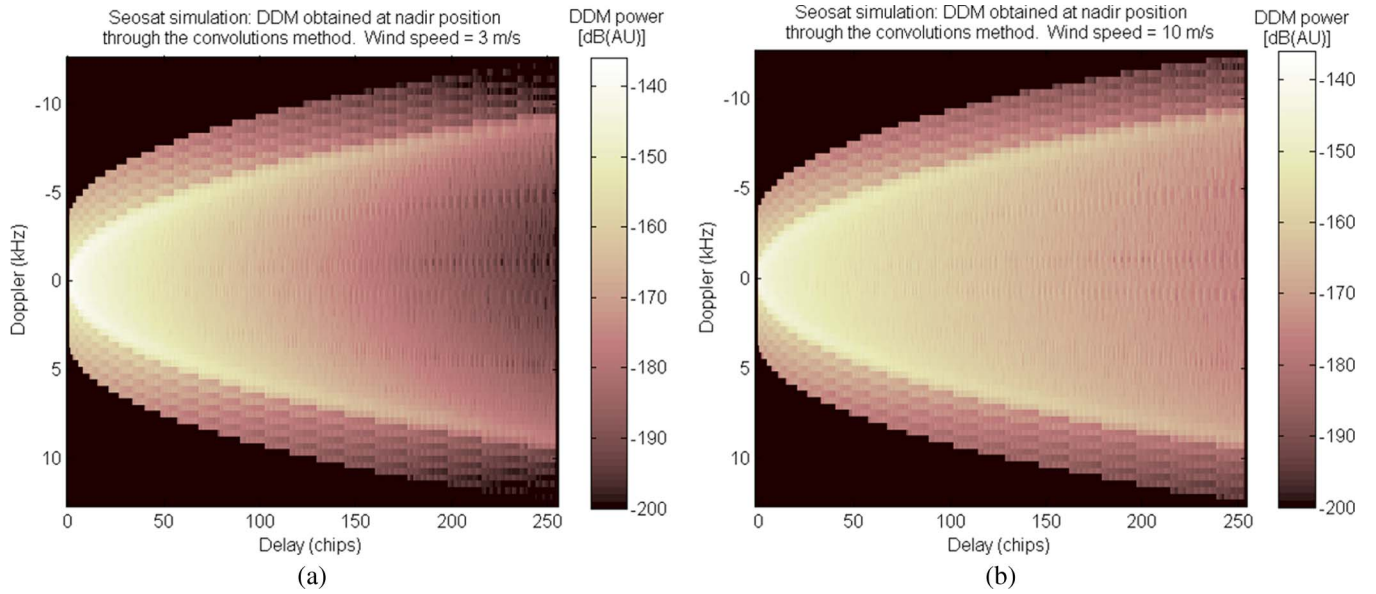


Fig. 2. Simulated DDMs (log-scale) when the GPS scattered signal is at nadir of the GNSS-R receiver ( $h = 681$  km) for wind speeds equal to (a) 3 m/s and (b) 10 m/s. A reduction of 4.5 dB (AU) for the peak power is observed (AU arbitrary unit).

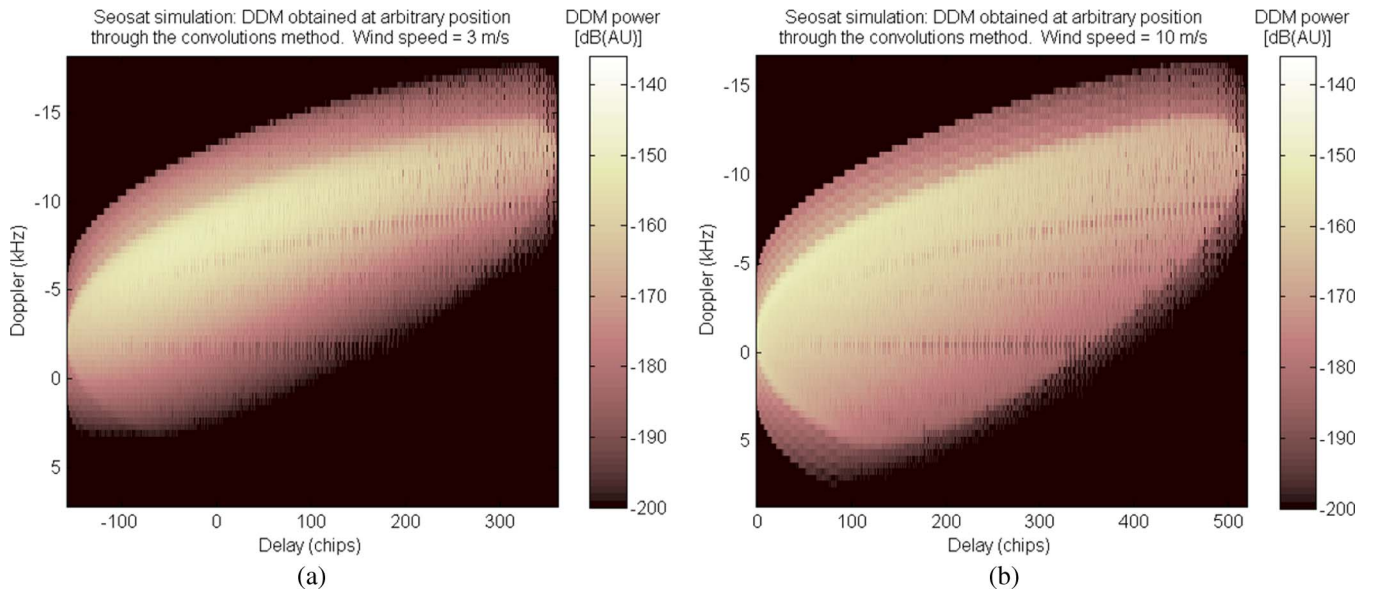


Fig. 3. Simulated DDMs (log-scale) when the GPS scattered signal is at the half-power beamwidth of the GNSS-R receiver ( $h = 681$  km) for wind speeds equal to (a) 3 m/s and (b) 10 m/s.

### III. RELATIONSHIP BETWEEN BRIGHTNESS TEMPERATURE AND DDM PARAMETERS

In order to relate the DDM with the brightness temperature change induced by the sea state ( $\Delta T_{B,p}(\theta, \vec{p})$ ), it is important to extract from the DDM some physically meaningful parameters that can be linked to this change. In this paper, it is proposed to use the volume under the normalized DDM, which increases with increasing roughness, since the region from which the signals are scattered enlarges, i.e.,

$$\text{Volume} = \int_{\tau_{\min}}^{\tau_{\max}} \int_{f_{d,\min}}^{f_{d,\max}} \overline{\text{DDM}}(\tau, f_d) \cdot d\tau \cdot df_d \quad (10)$$

where  $\tau_{\min}$ ,  $\tau_{\max}$ ,  $f_{d,\min}$ , and  $f_{d,\max}$  are the minimum and maximum values for the code offset and Doppler shift, respectively, and  $\overline{\text{DDM}}(\tau, f_d)$  is the normalized DDM. However, since the numerical computation of the volume requires an infinite domain of integration both in delay and Doppler (in practice, a very large one), it is proposed also to use the area of a section of the normalized DDM at a given threshold below the maximum, i.e.,

$$\text{Area} = \iint_{\overline{\text{DDM}}(\tau, f_d) > \text{threshold}} d\tau \cdot df_d. \quad (11)$$

This threshold must carefully be selected in order to provide maximum sensitivity to the geophysical parameters. The

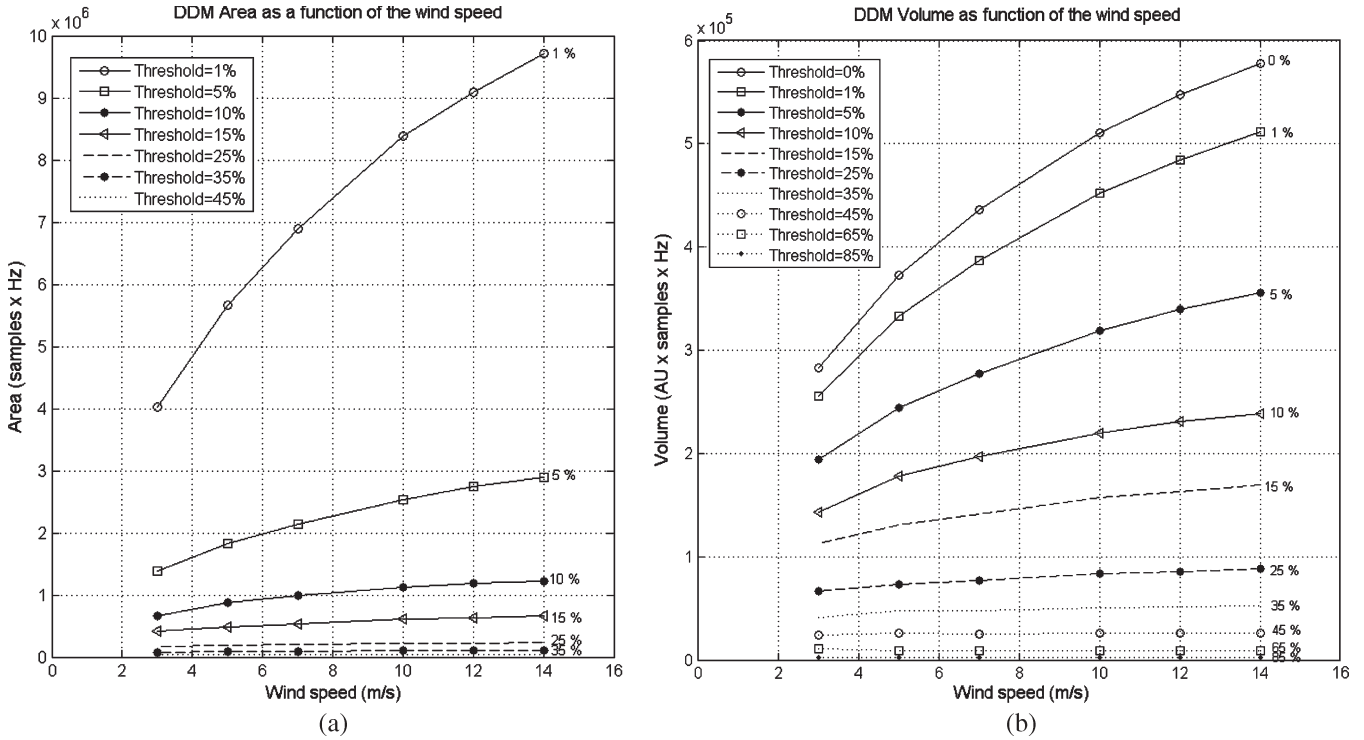


Fig. 4. (a) Area and (b) volume under the normalized DDM as a function of the wind speed and threshold used to compute them.

convention used in this paper is to define the threshold at a percentage of the maximum. For instance, a threshold of 10% from a normalized DDM would mean to consider only the points with amplitude over 0.1. The normalization is performed using the peak power of the DDM, so that its maximum is equal to one.

In order to study the relationship between the DDM volume or area and the sea state (in the set of simulations parameterized in terms of the wind speed only), a threshold at a given percentage of the maximum value has been defined, setting all points below it to zero. Fig. 4(a) and (b) shows the results for wind speeds from 0 to 14 m/s and different thresholds. The shape of the area also follows the same trend as the volume, and it is similar to that of the mean square slope versus wind speed [19], which suggests that both observables are also related to the same geophysical parameter. As expected, both the volume and the area decrease as the threshold increases, and the lower the threshold, the larger the sensitivity (largest output change for the same input change), with respect to the wind speed. Similarly, the  $\Delta T_{B,p}(\theta = 0^\circ, U_{10})$  (increase in the brightness temperature for the p polarization at nadir position as a function of surface wind speed  $U_{10}$ ) associated to the same roughness conditions was computed as described in [20]. It is then possible to link the DDM with the  $\Delta T_{B,p}(\theta = 0^\circ, U_{10})$ , which can be used to compensate for this term in the SSS retrieval algorithms. At present, this dependence is only empirically known with respect to the wind speed and/or the SWH [2], [3] or through models [21] that rely on the wind speed dependence (and eventually others such as the wave age [22] and other surface processes [23]). Even though  $\Delta T_{B,p}(\theta, V_{DDM})$  and  $\Delta T_{B,p}(\theta, A_{DDM})$  will only be known

when the DDMs and the brightness temperatures are simultaneously measured, an estimate can now be obtained by using the wind speed as intermediate variable  $\Delta T_{B,p}(\theta, V_{DDM}(U_{10}))$  and  $\Delta T_{B,p}(\theta, A_{DDM}(U_{10}))$ . This relationship is shown in Fig. 5(a) and (b), which have been obtained by replacing in Fig. 4(a) and (b) the wind speed dependence of the L-band brightness temperature at nadir derived using the small perturbation method/small slope approximation (SPM/SSA) [22], [24] (Fig. 6). This approach is one of the three algorithms implemented in the Soil Moisture and Ocean Salinity retrieval processor [25].

IV. PRACTICAL CONSIDERATION

The results presented in Fig. 5(a) and (b) assume a perfectly measured DDM in steps  $\Delta\tau = 1$  chip and  $\Delta f_d = 500$  Hz computed over a very large delay-Doppler region, so that the contributions of the tails outside the integration region are negligible. In this section, the following four aspects that appear in the practical implementation of the DDM generator are considered:

- 1) finite size in both the delay and Doppler variables:  $[\tau_{min}, \tau_{max}] \times [f_{d,min}, f_{d,max}]$ ;
- 2) DDM resolution: step width  $\Delta\tau$  and  $\Delta f_d$ ;
- 3) quantization of the DDM or the number of levels in which it is coded;
- 4) effect of the noise.

Since the sea state dependence is very similar both for the DDM area and the volume [Fig. 4(a) and (b)], in the remainder of this paper, only results for the DDM volume are presented.

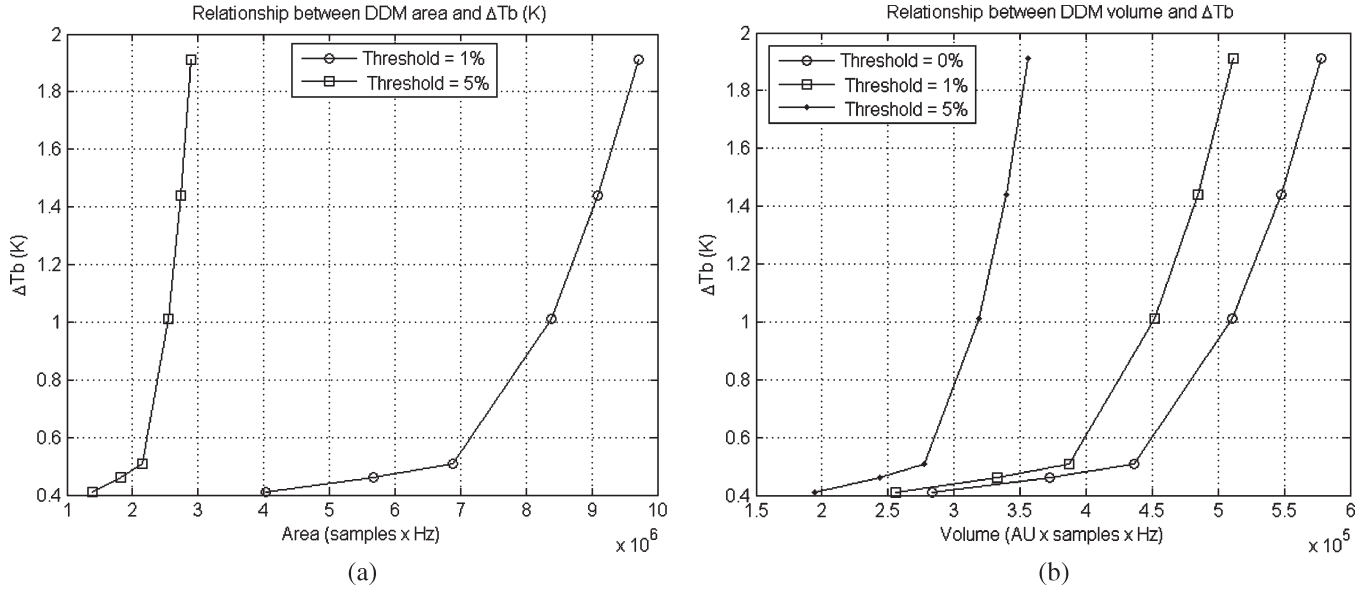


Fig. 5. Relationship between  $\Delta T_{B,p}(\theta = 0^\circ, \vec{p})$  and the (a) area and (b) volume under the normalized DDM.

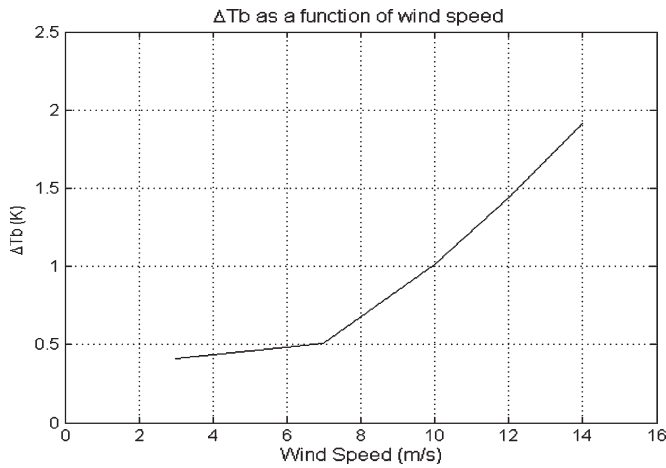


Fig. 6.  $\Delta T_B(\theta = 0^\circ, U_{10})$  as a function of the wind speed computed with the SPM/SSA method and the Elfouhaily's sea surface spectrum.

**A. DDM Finite Size**

From a practical point of view, it is convenient to reduce the size of the computed DDM, either using a field-programmable gate array [26] or in software after the signals are acquired. The idea is to find the minimum size around the DDM peak that provides an estimated area or volume close enough to the ideal case [Fig. 4(a) and (b)]. Results are shown in Fig. 7(a) and (b) for the estimated volume under the DDM. As expected, due to the widening of the DDM tails with increasing wind speed, the saturation occurs at higher delays, whereas the saturation Doppler frequency slightly increases. Consequently, the minimum DDM size, so that truncation errors are negligible, is 205 chips and  $\pm 11$  kHz ( $\leq 2\%$  error) for  $U_{10} = 10$  m/s and 220 chips and  $\pm 11$  kHz ( $\leq 2\%$  error) for  $U_{10} = 14$  m/s. This represents an area that is much larger than the antenna footprint, which is actually limiting the field of view from which reflections can be seen ( $\sim 260$  km). This footprint is compatible with

the size of the final salinity products to be derived, from 100 to 300 km of spatial resolution every 10 to 30 days [27], [28].

**B. DDM Resolution**

The DDM computation in real time is also limited by the number of points used to sample the DDM in each variable  $N_\tau = (\tau_{\max} - \tau_{\min})/\Delta\tau + 1$  and  $N_{f_d} = (f_{d,\max} - f_{d,\min})/\Delta f_d + 1$ . Therefore, the accuracy of the estimated area or volume of the normalized DDM is also affected by the DDM resolution.

The DDM is a wide and slow varying function, but under-sampling it results in a bias in the volume or area estimate, which translates into a bias in the estimated brightness temperature correction associated due to the sea state ( $\Delta T_{B,p}(\theta, \vec{p})$ ). To estimate this impact, the DDMs have been computed for several wind speed conditions decimating both in the delay and Doppler variables ( $\Delta\tau = N_{\text{decim. factor}, \tau}$  [in chips] and  $\Delta f_d = M_{\text{decim. factor}, f_d}$  [in hertz]), and results have been compared to those obtained using  $\Delta\tau = 1$  chip and  $\Delta f_d = 500$  Hz. Simulation results for the bias in  $\Delta T_{B,p}(\theta, \vec{p})$  as a function of the decimation factors  $N_{\text{decim. factor}, \tau}$  and  $M_{\text{decim. factor}, f_d}$  are shown in Fig. 8(a) and (b) for wind speeds of 3 and 10 m/s. In order to have a bias in the brightness temperature correction due to sea state that is smaller than, for example, 0.05 K ( $\sim 0.1$ -psu SSS error), the maximum decimating factors can be  $N_{\text{decim. factor}, \tau} = 1$  (1 chip) and  $M_{\text{decim. factor}, f_d} = 2$  (1 kHz).

**C. DDM Quantization**

The quantization of the DDM values into a finite number of levels results in roundoff errors that produce a bias in the area or volume estimate. Then, it translates into a bias in the brightness temperature correction to be applied due to the sea state. This bias decreases as the number of levels increases. The impact of the number of quantization levels in the DDM volume has been

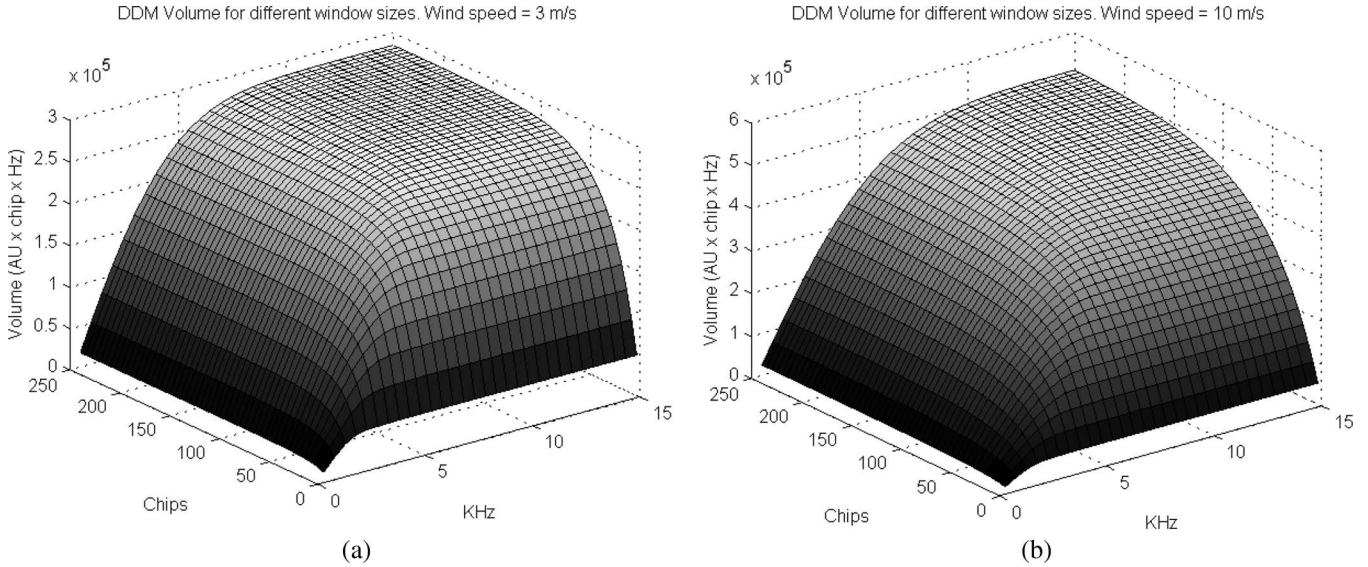


Fig. 7. Volume under the normalized DDM as a function of the normalized DDM size (chips  $\times$  kilohertz around the DDM maximum) for wind speed equal to (a) 3 m/s and (b) 10 m/s.

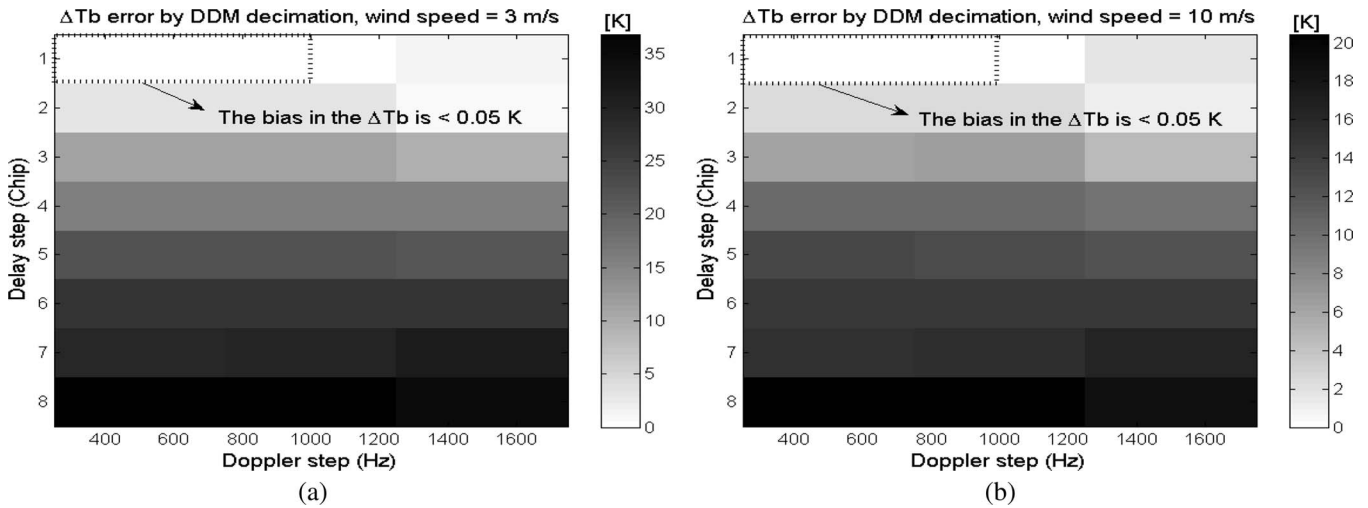


Fig. 8.  $\Delta T_{B,p}(\theta = 0^\circ, \vec{p})$  error as a function of the decimation factor in delay and Doppler frequency for wind speed equal to (a) 3 and (b) 10 m/s.

studied for wind speeds ranging from 3 to 14 m/s. Fig. 9(a) shows the bias in the DDM volume estimate as a function of the quantization levels from 2 (1 bit) to 1024 (10 bits). Fig. 9(b) shows the resulting bias in the brightness temperature correction. As it can be appreciated, for a bias smaller than 0.05 K, the number of levels must be larger than 256, and above 512, the bias is nearly independent of the sea state.

**D. Noise Impact**

In the previous sections, the effect of additive noise has not been taken into account. However, the performance of the brightness temperature correction ultimately depends on the amount of noise present in the DDMs. Taking into account that 1) the correlation time of the sea surface’s backscatter at L-band is on the order of a few milliseconds and 2) the possibility of having a sign change associated to the navigation bit, a 10-ms coherent integration time has been assumed, followed

by incoherent integration. In [29], the average noise level from a receiver in a low Earth orbit is given by

$$N = T_i^2 \left( \frac{K_p \cdot P + k_B T_{sys} B}{\sqrt{N_{incoherent}}} \right) \tag{12}$$

which includes two terms: 1) a speckle one, which depends on the scattered power  $P$  and  $K_p \approx 1/\sqrt{h}$ , which is related to the satellite height, and 2) a Gaussian thermal noise, which depends on Boltzmann’s constant  $k_B$ , system temperature  $T_{sys}$ , and system bandwidth  $B$ .

According to [29], the noise of the DDM module has a Rayleigh-Rice distribution since the noise in the real and imaginary parts are zero-mean Gaussian noises. This means that a noise increment increases not only the DDM variance but also its mean. This is a critical point since the brightness temperature correction ( $\Delta T_{B,p}(\theta, \vec{p})$ ) is computed through the DDM volume, which also increases with the noise level, resulting in a

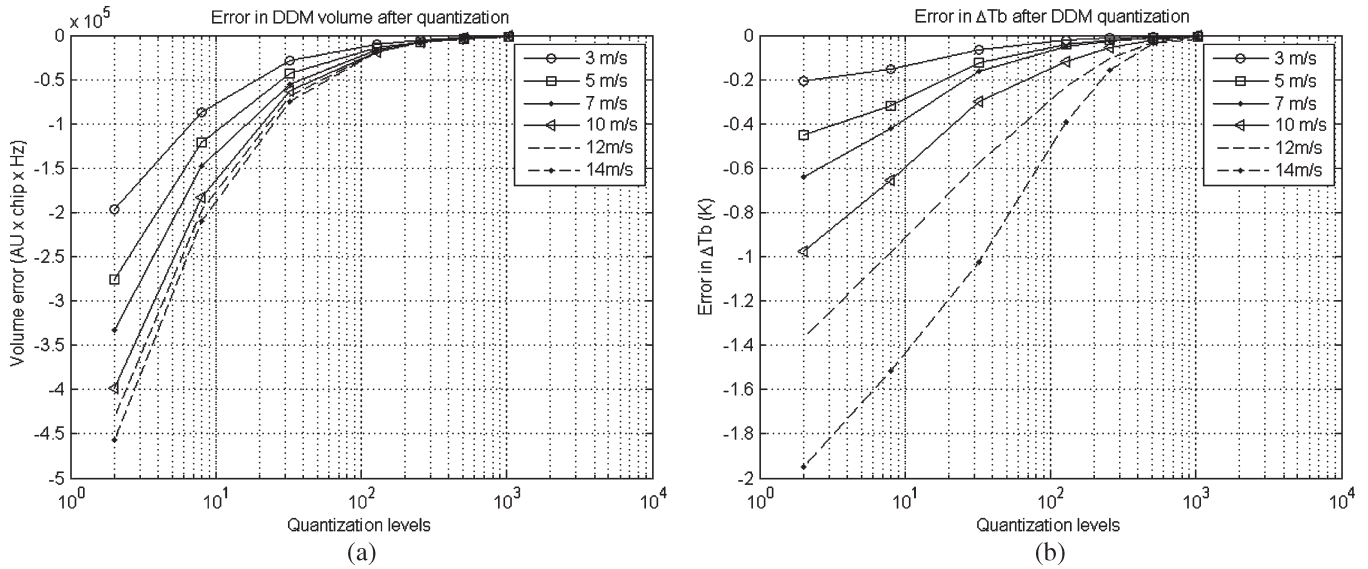


Fig. 9. Error in (a) estimated volume under the normalized DDM and (b) associated  $\Delta T_{B,p}(\theta = 0^\circ, \vec{p})$  error due to quantization.

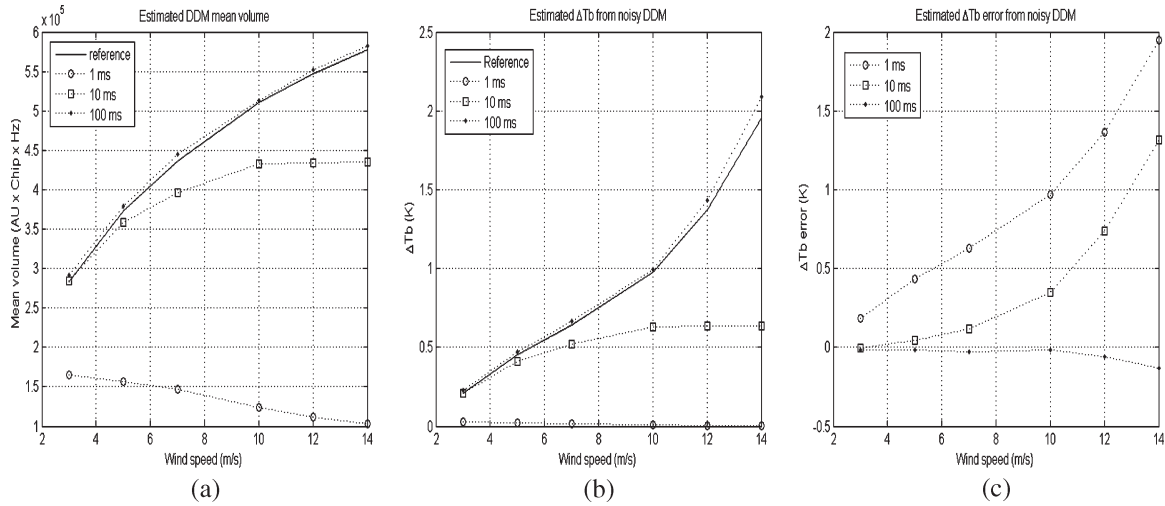


Fig. 10. (a) Estimated normalized DDM mean volume as a function of wind speed after subtraction of the estimated noise floor, (b) estimated  $\Delta T_{B,p}(\theta = 0^\circ, \vec{p})$ , and (c) associated error as a function of the wind speed. The DDM is computed for a coherent integration time of 1 ms and variable incoherent integration times of 1, 10, and 100 ms.

bias in  $\Delta T_{B,p}(\theta, \vec{p})$ . In order to compensate for this factor, the noise floor has to accurately be estimated. To do this, the mean value of the DDM points corresponding to “forbidden” delay-Doppler coordinates (coordinates that cannot exist for a given geometry, i.e., the dark blue regions in left of Figs. 2 and 3) is computed and then subtracted from the noisy DDM.

As shown in Fig. 10(a), the volume estimate improves as the incoherent integration time increases. Fig. 10(b) shows the values of estimated brightness temperature corrections for a coherent integration time of 1 ms and incoherent integration times of 1, 10, and 100 ms. Fig. 10(c) shows the associated error when comparing Fig. 10(b) with the noiseless ideal case. As it can be appreciated, the impact of noise increases with wind speed (sea state), and to achieve an error in the brightness temperature correction smaller than 0.05 K, the integration time must be 100 ms (1-ms coherent integration and 100-ms incoherent integration) for wind speeds below 11 m/s (at 14 m/s, this error is 0.13 K for the same incoherent integration time).

## V. CONCLUSION

This study, which was performed in view of the practical implementation of the GNSS-R processor of the PAU in the SeoSAT/INGENIO instrument proposal, has presented four results.

- 1) An efficient computation procedure to compute the DDMs of GNSS-R over the sea surface and collected by a satellite-borne receiver by means of 2-D convolutions.
- 2) The relationship between the area and volume under the DDM with respect to the wind speed used as the single descriptor of the sea state. This relationship has been used to link the brightness temperature correction due to the sea state, which was parameterized also in terms of the wind speed only, with the area or volume under the normalized DDM. This must be considered an intermediate step since the ultimate goal is to directly relate the area or volume under the DDM to the brightness

temperature correction, when measurements are available in the future.

- 3) Both the area and the volume as a function of the wind speed exhibit the saturation trend for higher wind speeds.
- 4) The requirements of the DDMs to be computed in order to accurately correct for the sea state impact on the L-band brightness temperature. These requirements are summarized as DDM size  $220 \text{ chips} \times \pm 11 \text{ kHz}$ , DDM resolution =  $1 \text{ chip} \times 1 \text{ kHz}$ , DDM quantization of at least 9 bits, and  $T_i = 1 \text{ ms}$  coherent integration, followed by 100-ms incoherent integration, assuming a GNSS-R receiver at 680-km height and a  $25^\circ$  beamwidth antenna.

Future research lines will include the evaluation of  $\Delta T_{B,p}(\theta, V_{\text{DDM}})$  and  $\Delta T_{B,p}(\theta, A_{\text{DDM}})$  for other bistatic scattering geometries since the relationship between sea roughness and the area/volume of the normalized DDM depends on the observation geometry (incidence angles, velocity vectors, etc.). In this paper, the area/volume and their link with roughness (and the subsequent brightness temperature increase) for the following particular geometry has been computed: GPS satellite exactly at the GNSS-R receiver's zenith and the velocities for both the emitter and the transmitter determined by the PAU/SeoSAT simulator. The generalization of the approach presented to an arbitrary scenario requires performing a set of simulations for each configuration.

## REFERENCES

- [1] J. Font, G. Lagerloef, D. LeVine, A. Camps, and O. Z. Zanife, "The determination of surface salinity with the European SMOS space mission," *IEEE Trans. Geosci. Remote Sens.*, vol. 42, no. 10, pp. 2196–2205, Oct. 2004.
- [2] A. Camps, J. Font, M. Vall-llossera, C. Gabarró, I. Corbella, N. Duffo, F. Torres, S. Blanch, A. Aguasca, R. Villarino, L. Enrique, J. Miranda, J. Arenas, A. Julià, J. Etcheto, V. Caselles, A. Weill, J. Boutin, S. Contardo, R. Niclós, R. Rivas, S. C. Reising, P. Wursteisen, M. Berger, and M. Martín-Neira, "The WISE 2000 and 2001 field experiments in support of the SMOS mission: Sea surface L-band brightness temperature observations and their application to multi-angular salinity retrieval," *IEEE Trans. Geosci. Remote Sens.*, vol. 42, no. 4, pp. 804–823, Apr. 2004.
- [3] C. Gabarró, J. Font, A. Camps, M. Vall-llossera, and A. Julià, "A new empirical model of sea surface microwave emissivity for salinity remote sensing," *Geophys. Res. Lett.*, vol. 31, no. 1, pp. L01 309.1–L01 309.5, Jan. 2004.
- [4] M. Martín-Neira, "A passive reflectometry and interferometry system (PARIS): Application to ocean altimetry," *ESA J.*, vol. 17, no. 4, pp. 331–355, Jan. 1993.
- [5] A. Rius, J. M. Aparicio, E. Cardellach, M. Martín-Neira, and B. Chapron, "Sea surface state measured using GPS reflected signals," *Geophys. Res. Lett.*, vol. 29, no. 23, p. 2122, Dec. 2002.
- [6] F. Soulat, M. Caparrini, O. Germain, P. Lopez-Dekker, M. Taani, and G. Ruffini, "Sea state monitoring using coastal GNSS-R," *Geophys. Res. Lett.*, vol. 31, no. 21, p. L21 303, Nov. 2004.
- [7] V. U. Zavorotny and A. G. Voronovich, "Scattering of GPS Signals from the ocean with wind remote sensing application," *IEEE Trans. Geosci. Remote Sens.*, vol. 38, no. 2, pp. 951–964, Mar. 2000.
- [8] R. N. Treuhaf, S. T. Lowe, C. Zuffada, and Y. Chao, "2-cm GPS altimetry over Crater Lake," *Geophys. Res. Lett.*, vol. 28, no. 23, pp. 4343–4346, Dec. 2001.
- [9] E. Cardellach, G. Ruffini, D. Pino, A. Rius, A. Komjathy, and J. L. Garrison, "Mediterranean balloon experiment: Ocean wind speed sensing from the stratosphere using GPS reflections," *Remote Sens. Environ.*, vol. 88, no. 3, pp. 351–362, Dec. 2003.
- [10] D. Masters, V. Zavorotny, S. Katzberg, and W. Emery, "GPS signal scattering from land for moisture content determination," in *Proc. Int. Geosci. Remote Sens. Symp.*, Honolulu, HI, 2000, pp. 3090–3092.
- [11] A. Komjathy, J. Maslanik, V. Zavorotny, P. Axelrad, and S. Katzberg, "Sea ice remote sensing using surface reflected GPS signals," in *Proc. Int. Geosci. Remote Sens. Symp.*, Honolulu, HI, 2000, pp. 2855–2857.
- [12] S. T. Lowe, J. L. LaBrecque, C. Zuffada, L. J. Romans, L. E. Young, and G. A. Hajj, "First spaceborne observation of an Earth-reflected GPS signal," *Radio Sci.*, vol. 37, no. 1, pp. 7–1–7–28, 2002.
- [13] S. Gleason, S. Hodgart, Y. Sun, C. Gommenginger, S. Mackin, M. Adjrard, and M. Unwin, "Detection and processing of bistatically reflected GPS signals from low Earth orbit for the purpose of ocean remote sensing," *IEEE Trans. Geosci. Remote Sens.*, vol. 43, no. 6, pp. 1229–1241, Jun. 2005.
- [14] J. B. Y. Tsui, *Fundamentals of Global Positioning System Receivers. A Software Approach*. New York: Wiley-Interscience, 2000.
- [15] M. Skolnik, *Radar Handbook*, 2nd ed. New York: McGraw-Hill, 1990.
- [16] A. Camps, X. Bosch-Lluis, J. F. Marchan-Hernandez, I. Ramos-Perez, B. Izquierdo, and N. Rodríguez-Alvarez, "New instrument concepts for ocean sensing: Analysis of the PAU-radiometer," *IEEE Trans. Geosci. Remote Sens.*, vol. 45, no. 10, pp. 3180–3192, Oct. 2007.
- [17] H. You, J. L. Garrison, G. Heckler, and V. U. Zavorotny, "Stochastic voltage model and experimental measurement of ocean-scattered GPS signal statistics," *IEEE Trans. Geosci. Remote Sens.*, vol. 42, no. 10, pp. 2160–2169, Oct. 2004.
- [18] S. Lowe, C. Zuffada, Y. Chao, P. Kroger, L. Young, and J. LaBrecque, "5-cm-precision aircraft ocean altimetry using GPS reflections," *Geophys. Res. Lett.*, vol. 29, no. 10, p. 1375, May 2002.
- [19] R. Sabia, M. Caparrini, A. Camps, and G. Ruffini, "Potential synergetic use of GNSS-R signals to improve the sea-state correction in the sea surface salinity estimation: Application to the SMOS mission," *IEEE Trans. Geosci. Remote Sens.*, vol. 45, no. 7, pp. 2088–2097, Jul. 2007.
- [20] J. J. Miranda, M. Vall-llossera, A. Camps, N. Duffo, I. Corbella, and J. Etcheto, "Sea state effect on the sea surface emissivity at L-band," *IEEE Trans. Geosci. Remote Sens.*, vol. 41, no. 10, pp. 2307–2315, Oct. 2003.
- [21] M. Vall-llossera, J. Miranda, A. Camps, and R. Villarino, "Sea surface emissivity modelling at L-band: An inter-comparison study," in *Proc. 1st Results Workshop EuroSTARSS, WISE LOSAC Camp.*, Nov. 4–6, 2002, pp. 143–153.
- [22] T. Elfouhaily, B. Chapron, K. Katsaros, and D. Vandermark, "A unified directional spectrum for long and short wind-driven waves," *J. Geophys. Res.*, vol. 102, no. C7, pp. 15 781–15 796, Jul. 1997.
- [23] B. Chapron, V. Kerbaol, D. Vandermark, and T. Elfouhaily, "Importance of peakedness in sea surface slope measurements and applications," *J. Geophys. Res.*, vol. 105, no. C7, pp. 17 195–17 202, Jul. 2000.
- [24] J. T. Johnson and M. Zhang, "Theoretical study of the small slope approximation for ocean polarimetric thermal emission," *IEEE Trans. Geosci. Remote Sens.*, vol. 37, no. 5, pp. 2305–2316, Sep. 1999.
- [25] C. Gabarró, M. Portabella, M. Talone, and J. Font, "Analysis of the SMOS ocean salinity inversion algorithm," in *Proc. Int. Geosci. Remote Sens. Symp.*, Barcelona, Spain, Jul. 23–27, 2007, pp. 971–974.
- [26] J. F. Marchán-Hernández, I. Ramos-Pérez, X. Bosch-Lluis, A. Camps, N. Rodríguez-Álvarez, and D. Albiol, "PAU-GNSS/R, a real-time GPS-reflectometer for Earth observation applications: Architecture insights and preliminary results," in *Proc. Int. Geosci. Remote Sens. Symp.*, Barcelona, Spain, Jul. 23–27, 2007, pp. 5113–5116.
- [27] G. S. E. Lagerloef, "Recent progress toward satellite measurements of the global sea surface salinity field," in *Satellites, Oceanography, and Society*, D. Halpern, Ed. Amsterdam, The Netherlands: Elsevier, 2000, pp. 309–319.
- [28] C. J. Koblinsky, P. Hildebrand, D. M. Le Vine, F. Pellerano, Y. Chao, W. J. Wilson, S. Yueh, and G. S. E. Lagerloef, "Sea surface salinity from space: Science goals and measurement approach," *Radio Sci.*, vol. 38, no. 4, p. 8064, 2003.
- [29] E. Cardellach, "Sea surface determination using GNSS reflected signals," Ph.D. dissertation, Univ. Politècnica de Catalunya, Barcelona, Spain, Dec. 2001.



**Juan Fernando Marchán-Hernández** (S'04) was born in Barcelona, Spain. He received the M.S. degree in telecommunications engineering from the Polytechnic University of Catalonia (UPC), Barcelona, in 2004. He is currently working toward the Ph.D. degree in the Passive Remote Sensing Group, Department of Signal Theory and Communications, UPC.

In 2003, he was with the Laboratory of Space Technology, Helsinki University of Technology (TKK), Espoo, Finland. His current research interests are radiometry and signal reflections of GNSS.



**Nereida Rodríguez-Álvarez** (S'07) was born in Barcelona, Spain. She received the M.S. degree in telecommunications engineering, in 2007, from the Universitat Politècnica de Catalunya (UPC), Barcelona, where she is currently working toward the Ph.D. degree in GNSS reflectometry.

She is currently with the Passive Remote Sensing Group, Department of Signal Theory and Communications, UPC.



**Xavier Bosch-Lluis** (S'04) was born in El Palau d'Anglesola, Spain. He received the M.S. degree in telecommunication engineering from the Universitat Politècnica de Catalunya, Barcelona, Spain, in 2005.

He was with the Passive Remote Sensing Group, Department of Signal Theory and Communications, Universitat Politècnica de Catalunya. He is currently with the Remote Sensing Laboratory, Universitat Politècnica de Catalunya. His research interests are L-band radiometry, digital beamforming, calibration techniques, and reflectometry of GNSS-R.



**Adriano Camps** (S'91–A'97–M'00–SM'03) was born in Barcelona, Spain, in 1969. He received the degree in telecommunications engineering and the Ph.D. degree in telecommunications engineering from the Universitat Politècnica de Catalunya (UPC), Barcelona, in 1992 and 1996, respectively.

During 1991–1992, he was with the Ecole Nationale Supérieure des Télécommunications de Bretagne, Brittany, France, with an Erasmus Fellowship. In 1993, he was with the Electromagnetic and Photonics Engineering Group, Department of Signal

Theory and Communications, UPC, as an Assistant Professor, and has been an Associate Professor since 1997. He is also a member of the Microwave Radiometry Group at UPC. In 1999, he was on sabbatical leave at the Microwave Remote Sensing Laboratory, University of Massachusetts, Amherst. He is an Associate Editor for *Radio Science*. His research interests include microwave remote sensing, with special emphasis on microwave radiometry by aperture synthesis techniques.

Dr. Camps was the Chair of  $\mu$ Cal 2001. From 2003 to 2006, he was Editor for the IEEE GEOSCIENCE AND REMOTE SENSING NEWSLETTER and the President–Founder of the IEEE Geoscience and Remote Sensing Society Chapter in Spain. He has performed numerous studies within the frame of the European Space Agency SMOS Earth Explorer Mission that have received several awards. He was the recipient of the Second National Award of University Studies in 1993; the INDRA Award of the Spanish Association of Telecommunication Engineering for the best Ph.D. in remote sensing in 1997; the Extraordinary Ph.D. Award at UPC in 1999; the Research Distinction of the Generalitat de Catalunya for contributions to microwave passive remote sensing in 2002; the European Young Investigator Award in 2004; and the 1st Duran Farell and the Ciudad de Barcelona awards for Technology Transfer, and the “Salvà i Campillo” Award of the Professional Association of Telecommunication Engineers of Catalonia for the most innovative research project in 2000, 2001, and 2004.



**Isaac Ramos-Pérez** (S'04–A'06) was born in Barcelona, Spain. He received the M.S. degree in telecommunications engineering, in 2005, from the Universitat Politècnica de Catalunya (UPC), Barcelona, where he is currently working toward the Ph.D. degree in microwave radiometry, developing a synthetic aperture passive advanced unit, i.e., a new instrument to develop and test potential improvements for future SMOS operational systems.

He was with the Passive Remote Sensing Group, Department of Signal Theory and Communications.



**Enric Valencia** (S'07) was born in Sabadell, Spain. He received the M.S. degree in electronic engineering, in 2007, from the Universitat Politècnica de Catalunya (UPC), Barcelona, where he is currently working toward the Ph.D. degree in GNSS reflectometry.

He is currently with the Passive Remote Sensing Group, Department of Signal Theory and Communications, UPC.